

Chiral phase transition and baryon number conservation

G. Holzwarth *

Fachbereich Physik, Universität-GH-Siegen, D-57068 Siegen, Germany

(June 1997)

Abstract

In the standard R^4 embedding of the chiral $O(4)$ model in 3+1 dimensions the winding number is not conserved near the chiral phase transition and thus no longer can be identified with baryon number. In order to reestablish conserved baryon number in effective low-energy models near and above the critical temperature T_c it is argued that insisting in $O(N)$ models on the angular nature of the chiral fields with fixed boundary conditions restores conservation of winding number. For $N = 2$ in 1+1 dimensions it is illustrated that as a consequence of the angular boundary conditions nontrivial solutions exist which would be unstable in R^2 ; moving trajectories avoid crossing the origin; and time evolution of random configurations after a quench leads to quasistable soliton-antisoliton ensembles with net winding number fixed.

I. INTRODUCTION

Effective chiral field theories in terms of a unitary matrix field $U(\mathbf{x}, t) \in SU(N_f)$ are considered as appropriate tool for the study of hadronic physics at very low energies [1]. The chiral field U comprises the lowest pseudoscalar meson multiplet for N_f flavors as Goldstone bosons of the spontaneously broken chiral symmetry of QCD. A most attractive feature of these models is the possibility to identify baryon number B with the winding number [2]

$$B = \frac{1}{24\pi^2} \int \epsilon^{ijk} \text{tr} L_i L_j L_k d^3x, \quad L_i = U^\dagger \partial_i U, \quad (1)$$

that characterizes the map of compactified coordinate space onto the $SU(N_f)$ manifold of the chiral fields. This concept has a profound basis [3] in the anomaly structure of underlying QCD, and it has found many successful applications as efficient description for meson-baryon systems without explicit use of fermion fields. Specifically, for $N_f = 2$ flavors,

*e-mail: holzwarth@hrz.uni-siegen.d400.de

it is the nontriviality of the third homotopy group $\pi_3(SU(2))$ which allows for the existence of baryons as topological defects in the chiral pion field.

It is expected that with increasing temperature the spontaneously broken chiral symmetry gets restored, such that beyond a critical temperature the chiral condensate vanishes and the Goldstone bosons acquire dynamical mass. Numerous examples in condensed matter systems [4] show the decisive role of topological defects for the dynamics of phase transitions if spatial and internal dimensions allow for nontrivial homotopy groups. For the cooling process of hot hadronic matter the topological arguments have been used [5] to obtain estimates for the baryon-antibaryon yield along the lines of the Kibble [6] mechanism.

On the other hand, it is expected that near and above the critical temperature $T = T_c$ it may be important to allow for additional degrees of freedom. Apart from vector mesons it appears natural to include (for $N_f = 2$) the scalar partner of the pseudoscalar pions into a common chiral field $\Phi = (\sigma, \boldsymbol{\pi})$, and to relax the constraint to the $SU(2)$ 3-sphere $\sigma^2 + \boldsymbol{\pi}^2 = f_\pi^2$. Thus the $SU(2) \times SU(2)$ -symmetric nonlinear σ model is replaced by the $O(4)$ -symmetric linear σ -model [7], where the fields $(\sigma, \boldsymbol{\pi})$ can freely explore the full 4-dimensional chiral space. This allows for a very convenient description of chiral symmetry restoration at finite temperatures [8], to study critical fluctuations of the chiral condensate near the phase transition, or to follow the dynamical formation of the condensate after a quench. It has been suggested that the exponential growth of collective amplitudes in the dynamical evolution of chiral field configurations after a quench may lead to disoriented chiral condensates in macroscopic regions of space [12] - [20]. These considerations have been based [17] - [20] on calculations within the framework of the $O(4)$ model [7] with chiral fields embedded in the simply connected R^4 internal space.

Unfortunately, with the unconstrained embedding of the chiral field Φ into a simple R^4 manifold the concept of baryon number B as winding index of topological defects is lost because the topological connectedness of this manifold is trivial. Of course, also in this embedding we may find nontrivial defect solutions which correspond to local minima in the energy hypersurface. Although they may be separated from the vacuum configuration $\sigma \equiv f_\pi, \boldsymbol{\pi} \equiv 0$ by a potential barrier which prevents their decay within classical dynamics, they no longer are topologically protected against decay into mesonic fluctuations. Cohen [9] has argued that the corresponding quantum mechanical tunneling amplitude vanishes in tree approximation in the limit where the number of colors $N_c \rightarrow \infty$. But a possible suppression for finite N_c through quantum corrections to our knowledge has never been proven. By suitable changes in the parameters of the model (e.g. by increasing the temperature) the decay process becomes even classically allowed.

Of course, we cannot have baryon number violated just by increasing the temperature. Apparently, we have to conclude that within the linear σ -model it makes no sense to identify winding number with baryon number. That conclusion, however, is quite unsatisfactory: it would imply that we have lost a fundamental symmetry of QCD in a model which we consider the appropriate tool for the study of hadronic physics near T_c . We would naturally expect that in cooling a hot hadronic plasma baryon-antibaryon production rates depend crucially on respecting this symmetry.

To avoid the above conclusion it would be desirable to combine the attractive features of the $O(4)$ model with the topological advantage of the nonlinear σ -model. The decisive feature is the angular nature of the chiral field. It is well known (see e.g. the discussion

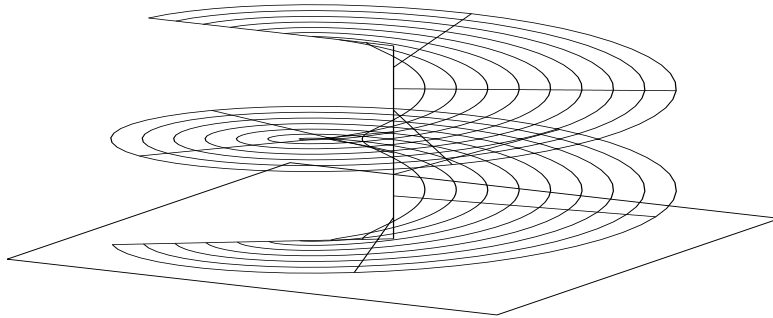


FIG. 1. Schematic view of two different manifolds which we consider as embeddings for the chiral $O(2)$ model: the R^2 plane spanned by cartesian components (σ, π) , and the angular $S^1 \times R^1$ manifold spanned by the radial and angular coordinates (r, ϕ) with its different sheets for the illustrative purpose pulled apart in vertical direction.

in [10]) that to specify an action in the continuum limit is not sufficient to fully specify a model. Additionally, the nature of the variables (continuous or periodic) must be specified on physical grounds. In our case it is baryon number conservation which therefore requires embedding the linear σ -model into the $S^3 \times R^1$ manifold as natural extension of the nonlinear σ -model, in contrast to the commonly used R^4 embedding. This means to insist on the angular nature of the chiral fields, i.e. on the factorization

$$\Phi = R(\mathbf{x}, t)U(\mathbf{x}, t), \quad (U \in SU(2)). \quad (2)$$

where the unitary part U as usual is parametrized by three chiral angles $\alpha(\mathbf{x}, t), \beta(\mathbf{x}, t), \gamma(\mathbf{x}, t)$

$$U = \exp(i \gamma \boldsymbol{\tau} \cdot \hat{\boldsymbol{\phi}}), \quad \hat{\boldsymbol{\phi}} = (\cos \alpha \sin \beta, \sin \alpha \sin \beta, \cos \beta). \quad (3)$$

This generates a discrete set of different continuous manifolds of angles α, β, γ which all describe the vacuum configuration $U = 1$ which the field must approach at spatial infinity $|\mathbf{x}| \rightarrow \infty$. They constitute distinct sets of boundary conditions for field configurations with finite energy and definite winding number. (In the plain R^4 embedding it is not possible to distinguish these different boundary conditions). As long as one of those boundary conditions is held fixed during the time evolution, the winding number as defined in (1) is conserved while the field Φ can explore the manifold $S^3 \times R^1$ without any further constraint. Thus identification of B with baryon number is meaningful.

Whenever a field configuration $\Phi(\mathbf{x}, t)$ (which we shall briefly call a 'trajectory') at some point in space and time acquires the value $\Phi = 0$, i.e. if a trajectory moves across the origin $R = 0$, the angular fields will jump by multiples of π . With boundary conditions on the angular fields fixed during the time evolution, this cannot happen, therefore trajectories will not be able to move across the origin and curled-up configurations will not be able to unwind by crossing the origin. It is, however, not necessary to enforce this by a constraint on R , or

by a singularity of the potential at the origin. It is enforced by the boundary conditions on the angular fields alone and reflects the fact that in the $S^3 \times R^1$ manifold the origin $R = 0$ as a highly singular branching point is excluded.

One may ask how this will affect the time evolution of trajectories which move according to the standard action of the $O(4)$ model. Ideally, without any damping mechanism, continuous trajectories moving across the origin will develop hairpin slings which tie them to the origin and serve to satisfy the angular boundary conditions, but do not otherwise affect the motion of the trajectories. In a real cooling process, however, all fluctuations are subject to dissipative damping which will be especially efficient for the high Fourier components of the slings. As a result, different embeddings will lead to different final configurations, irrespective of the precise nature of the dissipative mechanism.

Due to their topological equivalence the 1+1 dimensional $O(2)$ model can serve as a transparent illustration for the effects we may expect in the 3+1 dimensional $O(4)$ model. In the following sections we discuss some typical aspects: in sect.II we compare in angular and cartesian embedding the motion across the origin for very simple trajectories without and with potential ; in sect.III we determine the classical stable configurations and we show how the angular boundary conditions stabilize nontrivial solutions which collapse in the usual R^2 embedding to a point; finally, in sect.IV, we follow the time evolution of random initial configurations after a quench.

II. MOTION OF TRAJECTORIES IN DIFFERENT EMBEDDINGS

For the case of the 1+1 dimensional $O(2)$ model the two different embeddings are easily visualized: in the usual R^2 embedding the two-component chiral field $\Phi = (\sigma, \pi)$ lives on the R^2 plane spanned by cartesian components $-\infty < \sigma < \infty, -\infty < \pi < \infty$. The origin is naturally included without any singularity. The angular $R^1 \times S^1$ embedding in radial and angular variables ($0 < r < \infty, -\infty < \phi < \infty$)

$$\sigma(x, t) = r(x, t) \cos \phi(x, t), \quad \pi(x, t) = r(x, t) \sin \phi(x, t) \quad (4)$$

creates a manifold which consists of multiple sheets tied together at the origin $r = 0$ as branching point, like the Riemann sheets of the complex plane. This is illustrated in fig.1 which schematically shows the R^2 plane and the $R^1 \times S^1$ manifold with the different sheets pulled apart in vertical direction. Imagine a path embedded in the $R^1 \times S^1$ manifold connecting two points which differ in ϕ by 2π . Its projection into the R^2 plane is a closed loop which can be contracted to a point. But, evidently, with the endpoints fixed, the path on the angular manifold cannot be pulled across the origin and thus cannot be reduced to a point.

Specifically, let the discrete manifold

$$r = f_\pi, \quad \phi = n2\pi, \quad (5)$$

(n integer) represent an infinite set of distinct degenerate vacua. Choosing for a trajectory $\Phi(x, t)$ fixed boundary conditions $\phi(\pm\infty, t) = 2\pi n_\pm$ fixes the net winding number B

$$B = \frac{1}{2\pi} \int_{-\infty}^{\infty} \frac{\partial}{\partial x} \phi(x, t) dx = n_+ - n_-, \quad (6)$$

so that identification of B with conserved 'baryon number' is possible.

On the other hand, in the cartesian R^2 embedding all field configurations with boundary conditions

$$\sigma(-\infty, t) = \sigma(+\infty, t) = f_\pi, \quad \pi(-\infty, t) = \pi(+\infty, t) = 0, \quad (7)$$

represent closed loops in the σ - π plane which can be contracted continuously into the unique vacuum configuration $\sigma \equiv f_\pi, \pi \equiv 0$ and the integral (6) changes by one unit whenever the loop is pulled across the origin of the σ - π plane.

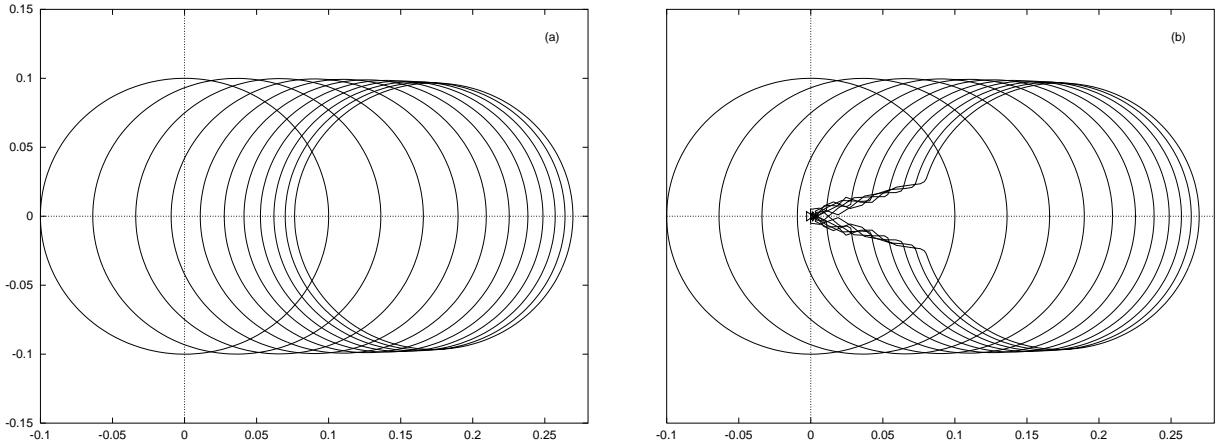


FIG. 2. Free motion of a circular trajectory with radius $r = 0.1$ across the origin (with small damping) in (a) R^2 and in (b) $S^1 \times R^1$ embedding of the $O(2)$ model.

As a most simple example let us consider the time evolution of a circular string moving to the right with a constant initial velocity across the origin in the absence of any potential. So the underlying Lagrangian density simply is

$$\mathcal{L}_0(\Phi) = \frac{1}{2} \partial_\mu \Phi \cdot \partial^\mu \Phi. \quad (8)$$

In 'cartesian' form the equations of motion are¹

$$\ddot{\sigma} = \sigma'' - \dot{\sigma}, \quad \ddot{\pi} = \pi'' - \dot{\pi} \quad (9)$$

with boundary conditions $\pi(-\infty, t) = \pi(+\infty, t) = 0$, and in 'angular' form

$$\ddot{r} = r'' - r(\dot{\phi}'^2 - \dot{\phi}^2) - \dot{r}, \quad \ddot{\phi} = \phi'' + \frac{2}{r}(r'\dot{\phi}' - \dot{r}\dot{\phi}) - \dot{\phi} \quad (10)$$

¹In the following x and t denote dimensionless spacetime variables. Where numbers are given, space and time are measured in units of the inverse physical pion decay constant of 93 MeV.

with boundary conditions $\phi(-\infty, t) = 0$, $\phi(+\infty, t) = 2\pi$. In both sets of differential equations the same dissipative terms (linear in the first time-derivatives) have been added to smoothen fluctuations which build up in the 'angular' parametrization. The effect of the dissipative terms can be seen in both cases as slowing down the translational motion. Figures 2a,b show the same ten consecutive equal time steps in a numerical evolution in the σ - π plane (a) and in the r - ϕ manifold (b). Evidently, as consequence of the topological constraint in case (b) the circular trajectory after crossing the origin drags behind it a tail of fluctuations, their precise form depending on mesh and damping details.

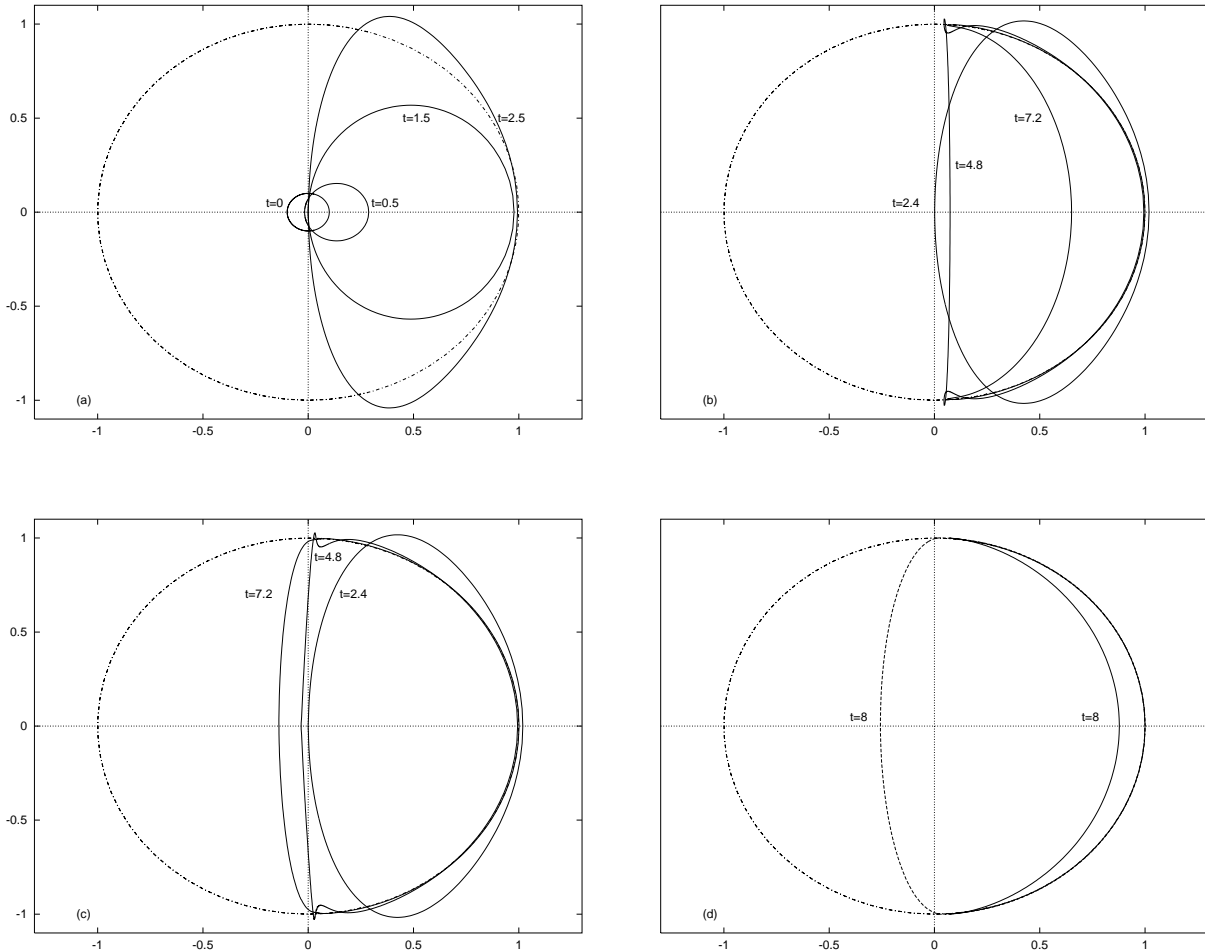


FIG. 3. Evolution of an initially small circular trajectory with radius $r = 0.1$ (moving with constant initial velocity as in fig.2) in the potential (11), in R^2 and in $S^1 \times R^1$ embedding: Up to $t = 2.5$ both evolutions coincide (a); (b) shows the further cartesian evolution for $t = 2.4, 4.8, 7.2$; (c) shows the angular evolution at the same time steps; in (d) both configurations are compared at $t = 8$ (full line: cartesian, dashed line: angular evolution). The dash-dotted circle denotes the bottom of the potential (in units of f_π).

Adding now to $\mathcal{L}_0(\Phi)$ the standard bell-shape potential

$$\mathcal{V}(\Phi) = \frac{\lambda}{4}(\Phi^2 - f_\pi^2)^2 \quad (11)$$

we may again in the two different manifolds follow the time evolution of the same circular trajectory (initial radius $r = 0.1f_\pi$ with constant initial velocity in positive σ direction) on the way to its final configuration located at the bottom of the well $r = f_\pi$. Up to the point where the trajectory meets the origin both evolutions are identical. While the left part of the circle is slowing down as it moves up towards the center top of the potential, the right half is rapidly accelerated downhill towards the bottom of the well. (Fig.3a shows the timesteps $t=0, 0.5, 1.5, 2.5$). In the σ - π evolution the left part then freely moves across the origin and follows the right half downhill into the same section of the bottom circle. (Fig.3b shows the timesteps $t=2.4, 4.8, 7.2$). In contrast to this, the r - ϕ evolution is held up at the origin and then slowly accelerated downhill on the left side of the well (fig.3c shows the same timesteps as fig.3b). Fig.3d shows both trajectories at time $t = 8$, where the right halves both have settled at the bottom $r = f_\pi$, the left part of the σ - π trajectory is approaching the bottom on the same side, while the left part of the r - ϕ trajectory is still moving downhill to complete after a few further timesteps the full circle which conserves the winding number of the initial $t=0$ configuration. Evidently, we can have with identical dynamics a dramatic difference of the evolutions in the different manifolds. Of course this only happens if the initial velocity is sufficient for the trajectory to overcome the center top of the potential. For smaller velocities both trajectories will evolve identically and both conserve winding number.

III. STABLE SOLITONS

The defects which carry winding number are not necessarily stable static configurations. Therefore, if their winding number is not topologically protected unstable defects will unwind and disappear. On the other hand, unstable topological defects will degenerate into spatially isolated singularities. It is therefore natural to expect that the stabilization mechanism of solitonic configurations will play an essential role for the evolution of trajectories.

In the 3+1-dimensional $O(4)$ -model soliton stabilization requires terms of higher chiral order, like the fourth-order Skyrme term [2]. The spatial extent of the angular chiral soliton profile scales as $(f_\pi e)^{-1}$ where the Skyrme parameter e remains essentially unchanged with increasing temperature. The angular winding length $L_w \sim f_\pi^{-1}$ as the characteristic length scale for stable field configurations then increases with increasing temperature. The radial bag with increasing L_w gets very shallow, i.e. $R(\mathbf{x})$ stays very close to f_π as f_π approaches zero with increasing temperature. So the static soliton dissolves together with restoration of chiral symmetry. But the baryon number defined through the choice of boundary condition in the $S^3 \times R^1$ embedding continues to be carried by the hot chiral gas even if the soliton has dissolved into chiral fluctuations around the vanishing mean value of the condensate.

It is nice to observe that also in the $O(2)$ model there is a simple way to destabilize static solitons and thus to choose any desired angular winding length. But unlike in the $O(4)$ case, here the mechanism is tied to explicit breaking of the $O(2)$ symmetry. Evidently, the static configuration

$$r = f_\pi, \quad \phi = B\pi(1 + x/L), \quad (12)$$

($2L$ is the size of the spatial box) which rests at the bottom of the well and winds B times

around the center, is stable for unbroken symmetry. It is also evident, that if we add a symmetry-breaking term $H\sigma$ to the potential

$$\mathcal{V}(\Phi) = \frac{\lambda}{4}(\Phi^2 - f^2)^2 - H\sigma. \quad (13)$$

there will be a maximal value of H which characterizes the onset of instability of static configurations with nonvanishing winding number. In order to keep the minimum of \mathcal{V} for finite H at $\Phi^2 = f_\pi^2$ we define

$$f^2 = f_\pi^2 - \frac{H}{\lambda f_\pi}. \quad (14)$$

The stable solitons correspond to bound trajectories of a classical point particle moving in the potential $-\mathcal{V}$, starting from the maximum of $-\mathcal{V}$ and returning to it after an infinite time. These configurations sling around the hat of the potential \mathcal{V} close to (but inside of) the bottom of the valley. Balancing centrifugal forces and potential gradient for such a classical particle provides the limiting value of H : stable solitons exist, as long as the inequality

$$\frac{H}{\lambda f_\pi^3} < 0.047 \quad (15)$$

is satisfied. In terms of σ - and π -masses

$$m_\pi^2 = \frac{H}{f_\pi}, \quad m_\sigma^2 = 2\lambda f_\pi^2 + m_\pi^2 \quad (16)$$

we find from (15) approximately $m_\sigma > 6.5 m_\pi$, as stability condition.

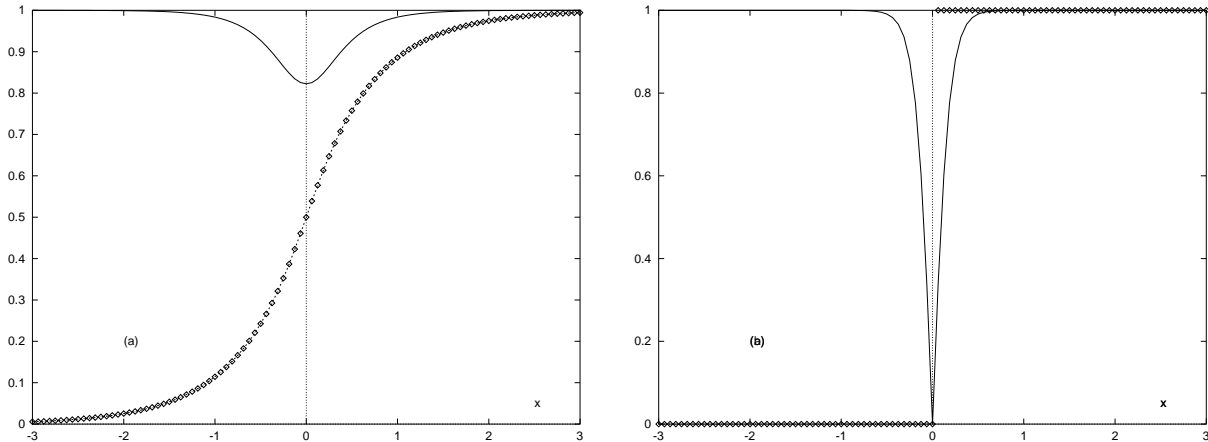


FIG. 4. Profiles of stable solitons in the $O(2)$ model ($m_\sigma = 1000$ MeV, $f_\pi = 93$) for two different values of m_π . In (a) $m_\pi = 140$ MeV is below, in (b) $m_\pi = 200$ MeV is above the critical value of $m_\sigma/6.5 = 154$ MeV. The full line is the radial bag profile $r(x)$ (in units f_π), the linespoints show the corresponding angular profiles $\phi(x)$ (in units of 2π). For $m_\pi > 154$ MeV ϕ is a step function.

The angular winding length $L_w \sim (\phi'(x=0))^{-1}$ (i.e. the inverse of the gradient of the angular field near the center of the soliton) defines the typical spatial extent of the stable soliton. In the symmetry limit $H \rightarrow 0$ $\phi(x)$ approaches $\pi(1+x/L)$, so in this limit the soliton completely occupies the spatial box of length $2L$. With increasing L_w the radial bag $r(x)$ gets very shallow, i.e. $r(x)$ stays very close to f_π .

Suppose that H , λ and f_π satisfy condition (15) for $T = 0$ and suppose we have a 'baryon' represented by a stable trajectory with $B = 1$. With increasing temperature T , the inclusion of loop corrections into a renormalized \mathcal{L} will lead to a decrease in $f_\pi^2(T)$ while the coupling constant λ and H remain unrenormalized. This causes the soliton radius to decrease. At a certain temperature the value of $H/(\lambda f_\pi^3)$ will exceed the critical stabilizing value (15), and in an R^2 embedding the sling will collapse to the vacuum point $\sigma \equiv f_\pi, \pi \equiv 0$, and the 'baryon' has disappeared.

If we repeat these considerations in the $S^1 \times R^1$ embedding starting with a stable trajectory at $T = 0$ with boundary conditions $\phi(-\infty, t) = 0, \phi(\infty, t) = 2\pi$, increase the temperature, then at the critical value (15) for $f_\pi(T)$ the sling will now collapse to a narrow hairpin around the origin which connects the vacua (5) with $n_- = 0$ and $n_+ = 1$, $\phi(x) = 2\pi\Theta(x)$. The radial field, however, still obeys a nonlinear equation

$$r'' - \lambda r(r^2 - f^2) + H = 0 \quad (17)$$

with nontrivial solutions satisfying

$$r(|x| \rightarrow 0) \rightarrow +0, \quad r(x \rightarrow \pm\infty) \rightarrow f_\pi - Ae^{-m_\sigma|x|}. \quad (18)$$

which represent the 'bag' profile of the remaining baryon with $B = 1$. Although its angular winding length L_w has shrunk to zero, the radial bag still has a nonzero radius in coordinate space which increases with temperature as long as the σ -mass decreases (in this particular stabilization mechanism which is peculiar to 1 space dimension). In fig.4 soliton profiles are shown for two values of m_π above and below the critical value (15). The stable soliton solutions above critical symmetry breaking do not exist in the R^2 embedding of this model.

IV. EVOLUTION AFTER A QUENCH

It is an interesting question to ask whether and how the topological aspects discussed above may affect the time evolution of chiral fields after a quench where an initially hot hadronic gas is rapidly cooled down across the chiral phase transition. The initial configuration therefore is characterized by an ensemble of randomly curled up trajectories which reflect the unbroken symmetry of the hot chiral gas phase. The time evolution of each trajectory after the quench then is governed by the equations of motion in the low temperature effective potential. In the commonly used R^4 embedding the initial configurations therefore can be created as random Gaussian ensembles centered around the origin $\Phi=0$ [18]. In the angular representation (2),(3) of the chiral fields this would correspond to uniform deviates in the three chiral angles

$$0 \leq \alpha \leq 2\pi, \quad 0 \leq \beta \leq \pi, \quad 0 \leq \gamma \leq \pi.$$

However, in $S^3 \times R^1$ embedding the chiral angles extend over all values $-\infty < \alpha, \beta, \gamma < +\infty$ and chiral symmetry requires equal probability for all values. So with each point of each trajectory all integer multiples of 2π should also be included. This implies that initial field configurations could curl arbitrarily often back and forth around the origin from one lattice point to the next, with only the net winding number B of the configuration inside the whole spatial box of radius L fixed. With our interpretation of the Jacobian

$$b(\mathbf{x}) = \frac{1}{2\pi^2} \sin \beta \sin^2 \gamma \frac{\partial(\alpha, \beta, \gamma)}{\partial(x, y, z)} \quad (19)$$

as local baryon density such configurations apparently should be very much suppressed.

Instead, for high values of the temperature T the initial ensemble should be such that the correlation function at $t = 0$ is characterized by a small correlation length $\xi_0 \sim T^{-1}$

$$\langle \text{tr } U^\dagger(\mathbf{x} + \mathbf{r}, 0) U(\mathbf{x}, 0) \rangle \sim e^{-|\mathbf{r}|/\xi_0}. \quad (20)$$

with dominant individual configurations characterized by a small local baryon density. With $\xi_0 \ll L$ such configurations again wind many times back and forth around the origin within the whole spatial box, but most of the phase differences between neighbouring lattice points should be less than 2π ,

Starting from such initial configurations, together with a Gaussian deviate in $R(\mathbf{x}, 0) > 0$ around $R = 0$, in $S^3 \times R^1$ embedding the growth of collective motion in radial direction towards the condensate cannot proceed (even for $B = 0$) through unwinding random multiple twists around the origin by moving the curled-up trajectories across the origin. Furthermore, while the evolution of the radial part $R(\mathbf{x})$ towards the condensate is driven by the slope of the potential $V(R)$, there is no corresponding driving force to unwind the large amplitude fluctuations in the angles α, β, γ . However, inclusion of dissipative terms will relax also the random angular fluctuations into a quasistable ensemble of B_+ solitons and B_- antisolitons (with $B = B_+ - B_-$) distributed randomly within the spatial box. Although the configuration then is characterized by a phase correlation length of order L_w it generally will contain many sections winding back and forth around the origin. Whether optimal unwinding ($B_+ = B$) can be achieved depends on the ratio of three different length scales: the initial phase correlation length ξ_0 (\sim the lattice constant), the winding length L_w of stable (anti)solitons i.e. on the stabilization mechanism, and on the size L of the box. A necessary condition for optimal unwinding is $\xi_0 \ll L_w$, because otherwise the initial configuration will be close to some quasistable soliton-antisoliton trajectory with comparable large mean square deviations $\sim L/\xi_0$ in the chiral angles. If $\xi_0 \ll L_w \ll L$, the quasistable trajectory can be very different from the initial incoherent fluctuations but still may contain many multiply curled-up sections. Only if L_w is comparable or larger than $L/(B + 2)$ then no stable soliton-antisoliton configurations fit into the box and the dissipative term can completely unwind all fluctuations. Of course, in all cases the net winding number B will be conserved. Because the different length scales change with temperature, the detailed study of the cooling process of the hot pion gas in this extended $S^3 \times R^1$ frame (as compared to [5]) might provide interesting features of baryon-antibaryon formation.

Again it is possible and illustrative to simulate such time evolutions in the $S^1 \times R^1$ $O(2)$ model. As discussed above the initial configurations should reflect the high value of

the temperature T through a small correlation length $\xi_0 \sim T^{-1}$ characterizing the angular correlation function at $t = 0$

$$\langle e^{i\phi(x_0+x,0)} e^{-i\phi(x_0,0)} \rangle = e^{-\frac{1}{2}\langle [\phi(x_0+x,0) - \phi(x_0,0)]^2 \rangle} = e^{-|x|/\xi_0}. \quad (21)$$

This shows that the mean square net winding increases linearly with x . On a lattice with lattice constant a this corresponds to a random walk with $|x|/a$ steps with a mean square step size of $2a/\xi_0$. Identifying ξ_0 with the lattice constant we obtain suitable initial configurations for the angles $\phi(x,0)$ by random walks with Gaussian deviate for mean square step sizes of order two, and fixed value of total net winding n . If $a \ll 2L$ these configurations wind many times back and forth around the origin, but most of the phase differences between neighbouring lattice points are less than 2π , i.e. the local baryon density $\sim \phi'(x,0)/(2\pi)$ is small. The actual value of the total winding number $B = n_+ - n_-$ of the configuration apparently is of minor importance for the general features of the evolution: as long as the field curls many times back and forth around the origin, it is not essential at which multiple of 2π it ends.

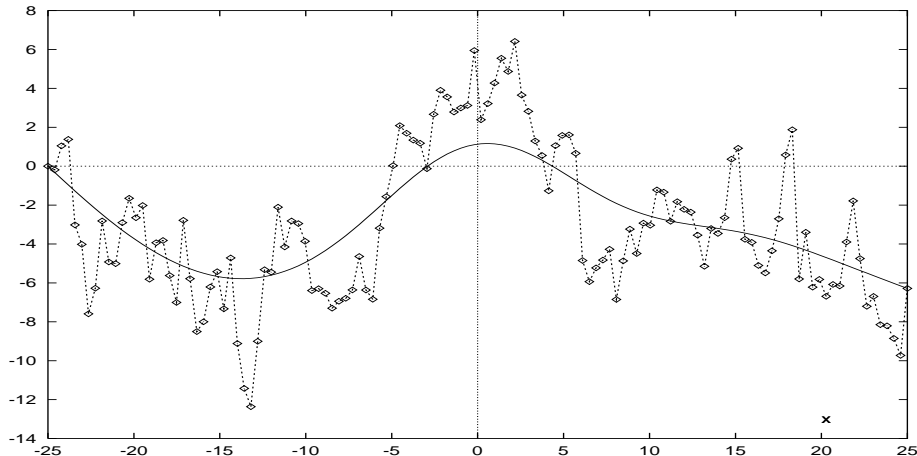


FIG. 5. The angular field ϕ at time $t = 20$ (full line) after evolving in the $S^1 \times R^1$ embedding of the $O(2)$ model from a random initial configuration $\phi(x, t = 0)$ (linespoints) for $m_\sigma = 1000$ MeV, $f_\pi = 93$, and no explicit symmetry breaking ($m_\pi = 0$).

As an illustration we consider the time evolution of an initial configuration on 128 lattice points in a box $-L \leq x \leq L$ ($L = 25$) which consists of a Gaussian deviate in the radial field $r(x)$ around the origin $r = 0$ and the angular configuration $\phi(x)$ given by a Gaussian random walk which begins at $\phi(-L) = 0$ and ends near $\phi(L) \approx -2\pi$ (cf. the linespoints in fig.5). In order to have integer B we put $\phi(L) = -2\pi$ and keep both boundary values $\phi(-L)$, $\phi(L)$ fixed for all times t . For a comparison with an evolution in R^2 embedding we obtain the corresponding cartesian initial configuration from (4) which then, of course, satisfies $\pi(-L) = \pi(L) = 0$. For the sake of our comparison we keep this boundary condition also fixed during the cartesian evolution.

The time evolution for $t > 0$ is governed by the potential (11). (We take $m_\sigma = 1000$ MeV and $f_\pi = 93$). Again we add dissipative terms in the equations of motion as in (9),(10). So, in angular form we have

$$\begin{aligned}
\ddot{r} &= r'' - r(\dot{\phi}^2 - \dot{\phi}^2) - \lambda r(r^2 - f^2) + H \cos \phi - \dot{r}, \\
\ddot{\phi} &= \phi'' + \frac{2}{r}(r'\phi' - \dot{r}\dot{\phi}) - \frac{H}{r} \sin \phi - \dot{\phi}
\end{aligned}
\tag{22}$$

Let us first consider the case of unbroken symmetry, i.e. $m_\pi = 0$. As we discussed in the previous section, in this case the slings (12) which rest at the bottom of the well and wind B times around the origin are stable classical solutions which finally will be approached by any evolution in time. The early phase ($t < 2$) of each evolution, angular or cartesian, is characterized by a rapid increase in the average radius of the trajectory towards the bottom of the well. During this early phase the cartesian trajectory crosses the origin repeatedly at different points in space and time with corresponding changes in net winding number B . In the following ($t < 10$) the evolutions are characterized by smoothing of the rapid random fluctuations. Finally, the remaining long-range variations of the trajectories are slowly reduced until finally the stable slings (12) are approached ($t > 100$).

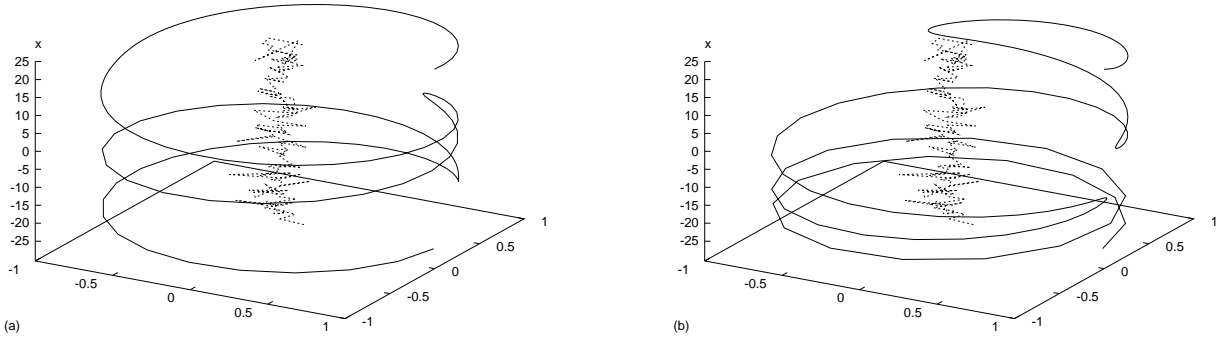


FIG. 6. Comparison between trajectories in the $O(2)$ model at time $t = 20$ after evolving in (a) $S^1 \times R^1$ and in (b) R^2 embedding from the same random initial configuration as in fig.5 (points connected by dashed lines near the center of the σ - π plane). The plots show the fields $\sigma(x)$ vs. $\pi(x)$ vs. the (vertical) coordinate x . The angular field $\phi(x)$ in (a) coincides with the full line in fig.5. In both cases the trajectories begin and end at the vacuum values $\sigma = 1$, $\pi = 0$, and the radial field $r(x)$ has settled near the bottom of the potential (11) at $r = 1$ (in units of f_π). ($m_\sigma = 1000$ MeV, $m_\pi = 0$, $f_\pi = 93$).

Fig.5 shows for the angular evolution the typical situation ($t = 20$) after the second phase: The rapid fluctuations of the ($t = 0$) random walk in the angle $\phi(x, t)$ (linespoints) are smoothed away, the resulting smooth curve (full line) still follows the average path of the random walk, necessarily always connecting the fixed boundary values and thus conserving the winding number ($B = -1$ in our example). The corresponding trajectories at the same point in time ($t = 20$) for both evolutions are compared in figs.6a,b. The radius of both configurations has settled already at the final limit $r = 1$ (in units of f_π), the angle of the angular evolution (a) (as shown in fig.5) curls several times back and forth around the origin with net winding -2π . In contrast to this the trajectory (b) of the cartesian evolution

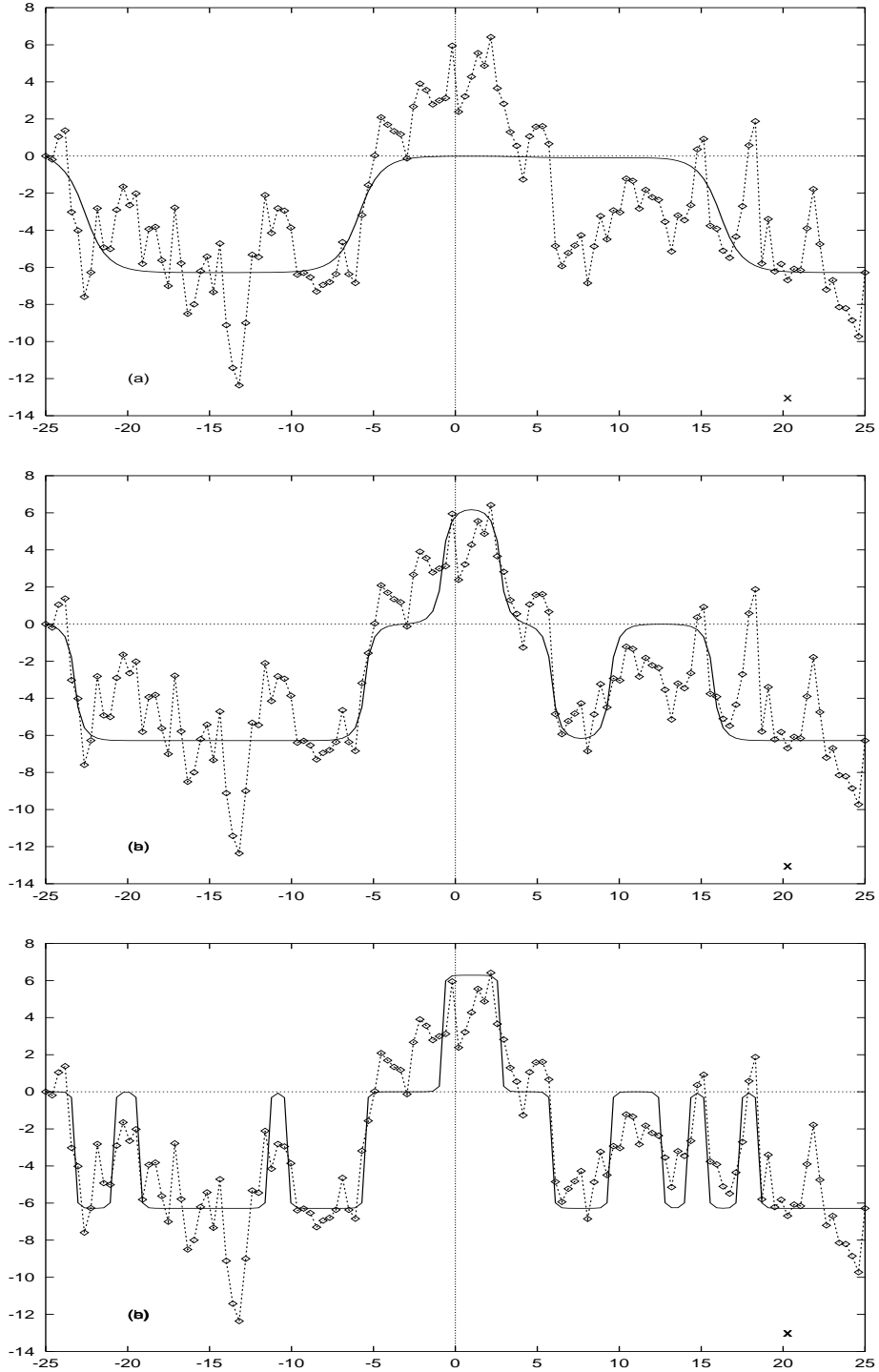


FIG. 7. The angular field $\phi(x, t)$ at time $t = 20$ (full lines) after evolving as in fig.5 in $S^1 \times R^1$ embedding of the $O(2)$ model from the same random initial configuration $\phi(x, t = 0)$ (linespoints) into quasistable soliton-antisoliton configurations $\phi(x, t = 20)$ for increasing symmetry breaking: (a): $m_\pi = 100$ MeV, (b): $m_\pi = 200$ MeV, (c): $m_\pi = 600$ MeV.

has at an early stage of the evolution suffered several changes of winding number and is approaching a final configuration with $B = +1$.

As discussed in the previous section, in this simple 1+1 dimensional model we have to break the $O(2)$ symmetry explicitly in order to destabilize the static solutions and allow for varying angular winding length L_w of the static solitons. From (15) the critical destabilizing value is $m_\pi = m_\sigma/6.5$ MeV, so for values $m_\pi > 154$ MeV the cartesian evolution rapidly ends at the trivial solution $\sigma = 1$, $\pi = 0$ with $B = 0$. For $m_\pi < 154$ MeV there is a chance for nonvanishing final values of B , but they are less likely because already in the very early stage of the cartesian evolution the broken symmetry drags the whole initial configuration across the origin towards the minimum of the potential.

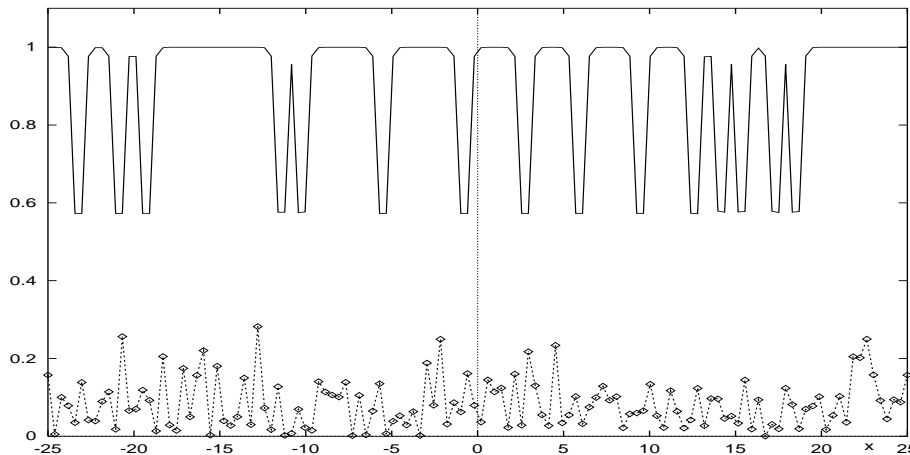


FIG. 8. The radial field $r(x, t)$ (in units of f_π) at time $t = 20$ after evolving in $S^1 \times R^1$ embedding of the $O(2)$ model from the random initial configuration $\phi(x, t = 0)$ (linespoints) as in figs.6 into the quasistable soliton-antisoliton configurations $r(x, t = 20)$ (full line) for strong symmetry breaking $m_\pi = 600$ MeV, corresponding to fig.7c.

In contrast to this, in the angular evolution B is conserved for all values of m_π and the decreasing angular winding length of the soliton solutions allows the evolution to approximate the original random fluctuations by an increasing number of metastable kink and antikink configurations. To demonstrate this effect we compare in figs.7a,b,c the angular field $\phi(x, t)$ resulting from the angular evolution at time $t = 20$ (as in fig.5) for three values of the symmetry-breaking 'pion' mass $m_\pi = 100, 200, 600$ MeV. For $m_\pi = 100$ MeV the angular field at time $t = 20$ has evolved into a $n_+ = 1$, $n_- = 2$ kink-antikink configuration shown in fig.7a which firmly rests in a local minimum of the energy hypersurface such that it does not evolve any further.

For m_π -values above 154 MeV we ideally expect a sequence of step functions in the angular distribution, while in the radial field the solitons still should have finite spatial extent (cf.(17)). This is shown in figs.7b,c for the angular evolution at time $t = 20$ with $m_\pi = 200$ and 600 MeV. Again the resulting configurations rest quasistable in local energy minima. In the numerical evolution due to the finiteness of the grid the kinks in the angle cannot really become step functions and the radial bags do not reach the value of $r = 0$ at their center (cf. fig.8). It is natural to expect that also in the continuum limit, when the

random walk initial configurations approach continuous differentiable functions the evolution will lead to trajectories which approximate these functions by a series of kinks and antikinks, or step functions (if the symmetry breaking exceeds the critical value (15)), with conserved net winding. Their local density will depend on the ratio of their winding length to the size of the box, and on the local gradients of the initial trajectory, i.e. on the initial local 'baryon' density.

V. CONCLUSION

In the commonly used R^4 embedding of the linear $O(4)$ σ model the angular nature of the chiral field is lost. As a consequence the winding number is not conserved and therefore no longer can be identified with baryon number, the latter concept being well established in the $SU(2) \times SU(2)$ nonlinear σ model.

For the early stages in the evolution of a hot hadron gas after a quench from the symmetric phase into the spontaneously symmetry-breaking cold phase this can be of crucial importance, because structures with nontrivial winding number contained in the random initial configurations can trivially unwind in the R^4 embedding and thus allow for the formation of large domains with uniform orientation of the chiral field. This has led to suggest spontaneous formation of macroscopic domains with differently oriented chiral condensates if the explicit symmetry breaking is sufficiently small.

On the other hand, in $S^3 \times R^1$ embedding, trajectories which are constrained by fixed boundary conditions on the angular variables cannot unwind and thus always reflect the net baryon number of the considered domain. Dissipative terms which must be present in the evolution equations will produce smooth trajectories which approximate the initial random angular configurations by random sequences of stable soliton and antisoliton structures. Their density depends crucially on the ratio of their angular winding length L_w to the size of the domain considered, but for sufficiently small L_w they closely reflect the local winding structure of the random initial configuration, as in the Kibble mechanism.

In the 1+1 dimensional $O(2)$ model used here for illustration the angular winding length of nontrivial soliton solutions is tied to explicit symmetry breaking. For $m_\pi = 0$ the final trajectories evolving after a quench interpolate linearly between the values $\phi(-L)$ and $\phi(L)$ at the boundaries of the domain with size $2L$. With explicit symmetry breaking these differ by multiples of 2π for sufficiently large domains. Small angular winding lengths L_w require large symmetry breaking. So the evolution of random initial configurations into soliton-antisoliton sequences within a given domain can be studied, but disoriented domains cannot be obtained within this simple model. This deficiency is absent in 3+1 dimensional $O(4)$ models where the mechanism which determines the angular winding length of nontrivial structures is largely independent of explicit symmetry breaking.

To summarize, if we want to maintain the topological concept of baryon number conservation in effective chiral theories near the chiral phase transition, we have to observe the angular nature of the chiral field and allow for a multitude of distinct sets of angles which describe the same physical situation. Partition functions in the usual R^4 embedding of the $O(4)$ model contain trajectories with fluctuating values of baryon number B with comparable weight, while the angular embedding allows to select also near and above T_c

only configurations with the same baryon number that characterizes the system at $T = 0$. This feature is a natural ingredient of the nonlinear σ model for pions and it should not be lost when the chiral partner of the pion is included as important degree of freedom near T_c .

ACKNOWLEDGMENTS

The author would like to thank H. Walliser, H. B. Geyer and F. Meier for many helpful discussions.

REFERENCES

- [1] S. Weinberg, *Physica* **96A**, 327 (1979); J. Gasser and H. Leutwyler, *Ann. Phys. (N.Y.)***158**, 142 (1984)
- [2] T. H. R. Skyrme, *Prog. R. Soc.* **A260**, 127 (1961);
- [3] E. Witten, *Nucl. Phys.* **B223**, 422 (1983), **B223**, 433 (1983).
- [4] see e.g.: G.E. Volovik, *Exotic Properties of Superfluid He³* (World Scientific, Singapore 1992); A. D. Rutenberg and A. J. Bray, *Phys. Rev. Lett.* **74**, 3836 (1995); W.H. Zurek, *Cosmological Experiments in Condensed Matter systems*, cond-mat/9607135.
- [5] J. Ellis and H. Kowalski, *Phys. Lett.* **B214**, 161 (1988); J. Ellis, U. Heinz, and H. Kowalski, *Phys. Lett.* **B233**, 223 (1989); J. Ellis, M. Karliner, and H. Kowalski, *Phys. Lett.* **B235**, 341 (1990).
- [6] T.W.B. Kibble, *J.Phys.***A9**, 1387 (1976).
- [7] M. Gell-Mann and M. Levy, *Nuovo Cimento***16**, 705 (1960).
- [8] G. Baym and G. Grinstein, *Phys. Rev.***D15**, 2897 (1977).
- [9] T. D. Cohen, *Phys. Rev.***D37**, 3344 (1988).
- [10] A.M.Polyakov, *Gauge Fields and Strings*, (Harwood Acad. Publ., Chur, 1987)
- [11] A. Bochkarev and J. Kapusta, *Phys. Rev.* **D54**, 4066 (1996).
- [12] A.A. Anselm, *Phys. Lett.* **B217**, 169 (1988); A.A. Anselm and M.G. Ryskin, *Phys.Lett.* **B266**, 482 (1991).
- [13] J.P. Blaizot and A. Krzywicki, *Phys. Rev.* **D46**,246 (1992); *Phys. Rev.* **D50**, 442 (1994).
- [14] J.D. Bjorken, *Int. J. Mod. Phys.* **A7**, 4189 (1992); *Acta Physica Polonica* **B23**, 561 (1992).
- [15] K.L. Kowalski and C.C. Taylor, *Disoriented chiral condensate: A white paper for the full acceptance detector CWRUTH-92-6* (1992), unpublished.
- [16] J.D. Bjorken, *Disoriented chiral condensate*, Proc. Workshop on Continuous advances in QCD, Minneapolis 1994, and SLAC-PUB-6488 (1994).
- [17] K. Rajagopal, in *Quark-Gluon Plasma 2*, ed. R. Hwa (World Scientific, 1995).
- [18] K. Rajagopal and F. Wilczek, *Nucl. Phys.* **B399**,395 (1993), **B404**,577 (1993).
- [19] S. Gavin, A. Gocksch and R.D. Pisarski, *Phys.Rev. Lett.* **72**, 2143 (1994).
- [20] M.A. Lampert, J.F. Dawson and F. Cooper, *Phys.Rev.* **D54**, 2213 (1996).